CHEMISTRY
A European Journal

A Journal of
ChemPubSoc Europe

Accepted Article

Title: Metallothermic Reduction of Silica Nanoparticles to Porous Silicon for Drug Delivery Using New and Existing Reductants

Authors: Yiqi Lai, Jonathan R. Thompson, and Mita Dasog

To be cited as: *Chem. Eur. J.* 10.1002/chem.201705818

Link to VoR: http://dx.doi.org/10.1002/chem.201705818

Supported by
ACES

WILEY-VCH

10.1002/chem.201705818

WILEY-VCH

FULL PAPER

Metallothermic Reduction of Silica Nanoparticles to Porous Silicon for Drug Delivery Using New and Existing Reductants

Yiqi Lai,[a] Jonathan R. Thompson,[b] and Mita Dasog*[a]

Abstract: In this study, the influence of metals (Mg, Al, and Ca) and reaction conditions (time, temperature, and metal grain size) on the metallothermic reduction of Stöber silica nanoparticles (NPs) to form porous Si was explored. Mg metal was found to be an effective reducing agent even at temperatures below its melting point; however, it also induced a high degree of structural damage and morphology change. Al was effective at reducing silica NPs only at its melting point and higher temperatures, but the resulting particles retained a higher degree of structural morphology as compared to those reduced using Mg. Ca was found to be ineffective in reducing silica. A new reductant, a mixture of 70% Mg and 30% Al, was found to induce the least amount of morphology change, and the reactions proceeded at temperatures (450 °C) lower than those required by Mg or Al individually. Furthermore, porous Si-NPs obtained using Mg, Al, and the mixture of 70% Mg and 30% Al as reductants were investigated as carriers for ibuprofen loading and release. Porous Si obtained from Mg and Mg/Al mixture reductions showed higher drug loading and a sustained drug release profile whereas porous Si obtained from Al reduction had lower loading and showed a conventional release profile over 24 hours.

Introduction

In the last two decades, porous Si has been extensively explored as an interesting optical material,[1-6] drug delivery vehicle,[7-11] sensor,[12-18] gas storage medium,[19,20] anode material for Li-ion batteries,[21-24] and in other energy conversion systems.[25-28] The utility of porous Si is highly dependent on the surface area, crystallinity, morphology, and pore volume, which are often dictated by the synthetic methods used to prepare them. Porous Si can be made using top-down approaches such as electrochemical etching[29-31] and metal-assisted chemical etching[32,33] or bottom-up approaches such as chemical vapor deposition,[8,34,35] carbothermal reduction,[36] and metallothermic reduction.[37-42] Among these methods, metallothermic reduction has gained significant attention as it allows for straightforward synthesis of porous Si from inexpensive precursors such as glass,[43] sand,[44-47] or sol-gel polymers.[38,39,48-50] Additionally, it allows for morphology retention and can be scaled up. The reducing metal of choice should be cheap, convenient to handle, produce an easily removable byproduct, have a relatively low melting point, and possess appropriate redox properties. Mg has been the most widely utilized metal for the reduction of Si oxide and suboxides as evidenced by the rapid growth in the number of publications in the last ten years. Other metals such as Al, Zn, Na, and K have also been explored for the reduction of silicon oxides and halides to form porous Si.[40,41,51-55] However, removal of alkali metal oxides can be hazardous due to their violent reaction with water. While Zn is known to react with Si halides to form porous Si, its reaction with silica is thermodynamically unfavorable.[53,54] Therefore, Mg and Al are more routinely utilized for the metallothermic reduction of silica.

Magnesiothermic and aluminothermic reduction reactions are performed at different temperatures, for varying lengths of time using different grain sizes of the metal. However, the effect of these variations or the choice of the metal on the physical properties of the resulting porous Si has not been systematically investigated. As the performance of porous Si based devices/systems are highly dependent on its physical properties, it is important to understand the influence of different reaction conditions on the resulting porous Si. For example, amorphous Si nanoparticles (NPs) perform better as a Li-ion anode material as compared to their crystalline counterparts.[56-58] However, crystalline Si-NPs perform better as photocatalysts due to fewer defect states.[26,59] Higher surface area allows for more reactivity with CO_2 or H_2O to form methanol and hydrogen fuel, respectively.[28,60] The nanostructuring of the porous Si, such as the volume of the void space or the size and 3-D arrangement of the primary particles, can influence the diffusion of Li-ions in batteries and the loading and unloading of drug molecules.[7,61-64] Porous Si for drug delivery and immunotherapy applications have predominantly been prepared *via* electrochemical etching. The etching parameters can control the pore size and particle morphology which in turn dictates the drug release kinetics in porous Si.[63] Typically, additional surface modification of Si surface or polymer encapsulation is required for sustained drug release in such systems.[8,65,66] Metallothermic reduction can offer an alternative scalable pathway to prepare drug delivery vehicles. However, better understanding of the influence of different metallothermic reduction reactions on loading and unloading of drug molecules in the resulting porous Si is necessary for its complete deployment.

Herein, we report the reduction of Stöber silica NPs with Mg, Al, and Ca metals. The influence of reaction temperature, time, and metal on the surface area, pore volume, crystallinity, and nano-

[a] Ms. Y. Lai and Prof. Dr. M. Dasog
Department of Chemistry
Dalhousie University
6274 Coburg Road, Halifax, NS, Canada
E-mail: mita.dasog@dal.ca
[b] Mr. J. R. Thompson
Division of Materials Science
California Institute of Technology
Pasadena, CA, United States

Supporting information for this article is given via a link at the end of the document.

10.1002/chem.201705818

structuring in porous Si was investigated. We further report a mixture of 70% Mg and 30% Al as a new low-temperature reductant. The performance of porous Si prepared with different metals was investigated as a carrier for ibuprofen loading and release experiments to demonstrate the difference in performance based on the synthetic method used.

Results and Discussion

Magnesiothermic reduction. Stöber silica NPs (238 ± 22 nm) were prepared using a previously reported base catalyzed sol-gel procedure (Figure S1).[67] They were mixed with -325 mesh Mg powder and NaCl salt which acted as a heat sink.[68,69] The reaction mixture was processed in a tube furnace under an Ar atmosphere at various temperatures and reaction lengths. The reduced product was treated with aqueous 1.0 M HCl solution to remove unreacted Mg, MgO, and NaCl. Figure 1 shows powder XRD patterns of the resulting product. At 500 °C the amount of Si increases with increasing reaction length, as evidenced by the decreasing intensity of the broad amorphous SiO_2 peak at 2θ ~ 22° and increasing intensities of peaks at 28.5°, 47.3°, and 56.1° corresponding to (111), (220), and (311) crystal planes of diamond structured Si, respectively.[48] This result is further confirmed from the XPS data (Figure S2), which shows the presence of only 10% elemental Si after 3 h reaction but the amount increases to ~75% after 24 h at 500 °C. At the melting point of Mg (650 °C), the reaction proceeds at a faster rate and ~70% elemental Si was observed after 3 h and reaches 90% after reacting for 24 h. A similar trend was observed in the XRD patterns of the products processed at 650 °C, where the SiO_2 peak intensity recedes with increasing reaction time. At 800 °C, about 82% elemental Si was formed within the first 3 h. While no SiO_2 reflection was observed in the XRD pattern, the maximum elemental Si obtained *via* magnesiothermic reduction remained at ~90% as determined with the XPS technique. It is possible for the surface oxidation to occur during the post-synthesis workup. The rate of formation of elemental Si slows down over time for all the temperatures investigated in this study. This is expected, as the diffusion path length in a solid-state reaction increases with more product formation, thereby slowing down the reaction rate.[70] The removal of byproducts was confirmed with the EDS technique (Figure S3) that showed a dominant peak originating from Si and also smaller peaks from Al originating from the sample holder and O which likely arises from the Si suboxides.

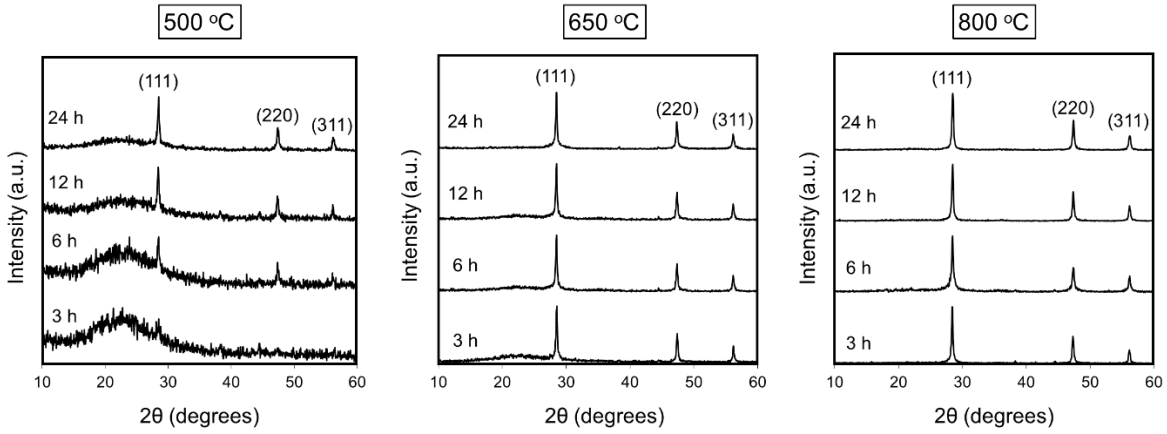

Figure 1. Powder XRD patterns of the products obtained *via* magnesiothermic reduction of Stöber silica NPs at 500, 650, and 800 °C for 3, 6, 12, and 24 hours.

Figure 2 shows representative SEM images of Mg reduced Stöber silica NPs. Significant loss of structural morphology was observed for the reaction products processed at 650 and 800 °C. While NaCl was added as a heat sink to all reaction mixtures, it is possible that the faster reaction rates at higher temperatures release higher amounts of heat in a given time interval, leading to more fracturing and the fusion of Si-NPs.

The surface area and pore volume of Stöber silica NPs were determined to be 8.2 m^2/g and 0.07 cm^3/g, respectively. The surface area of porous Si-NPs obtained at 500 °C and 6 and 12 h reaction times were 390 and 386 m^2/g, respectively (Figure S4). These surface areas were the highest of all the samples investigated. A pore volume of ~1.7 cm^3/g was determined and a pore size distribution (Figure S5) suggests pores with an average diameter of 10 nm for porous Si obtained at 500 °C and 12 h reaction time. The surface area decreased with increasing reaction temperature (Figure S4) consistent with the SEM images that show a higher degree of structural damage. This trend was further observed in the decrease in pore volume to 1.1 cm^3/g and 0.9 cm^3/g for 650 and 800 °C, respectively, 12 h reaction products. At 650 and 800 °C, an initial increase in surface area was observed after reacting for 12 h but decreased significantly after reacting for 24 h. Figure 3A shows a TEM of porous Si-NPs obtained at 650 °C after 12 h reaction time. The porous Si-NPs show a "blackberry-like" nanostructure made of smaller nanocrystals connected with each other in 3-D. A detailed

10.1002/chem.201705818

investigation of the fragments obtained from the damaged porous Si-NPs shows 30 – 70 nm Si structures (Figure 3B) which are likely formed by the high temperature fusion of smaller nanocrystals. The high resolution TEM shows characteristic lattice spacing for Si(111) plane, indicating that the fragments are crystalline in nature. The TEM contrast suggests these fragments to be non-porous. Given the exothermic nature of magnesiothermic reactions, it is possible for localized temperatures to reach above 1000 °C, leading to particle fusion.[69] As the processing temperature increases, the formation of such smaller fragments of Si also increases, leading to a decrease in surface area and pore volume. Individually detached 3 – 5 nm Si nanocrystals (Figure 3C) were also observed.

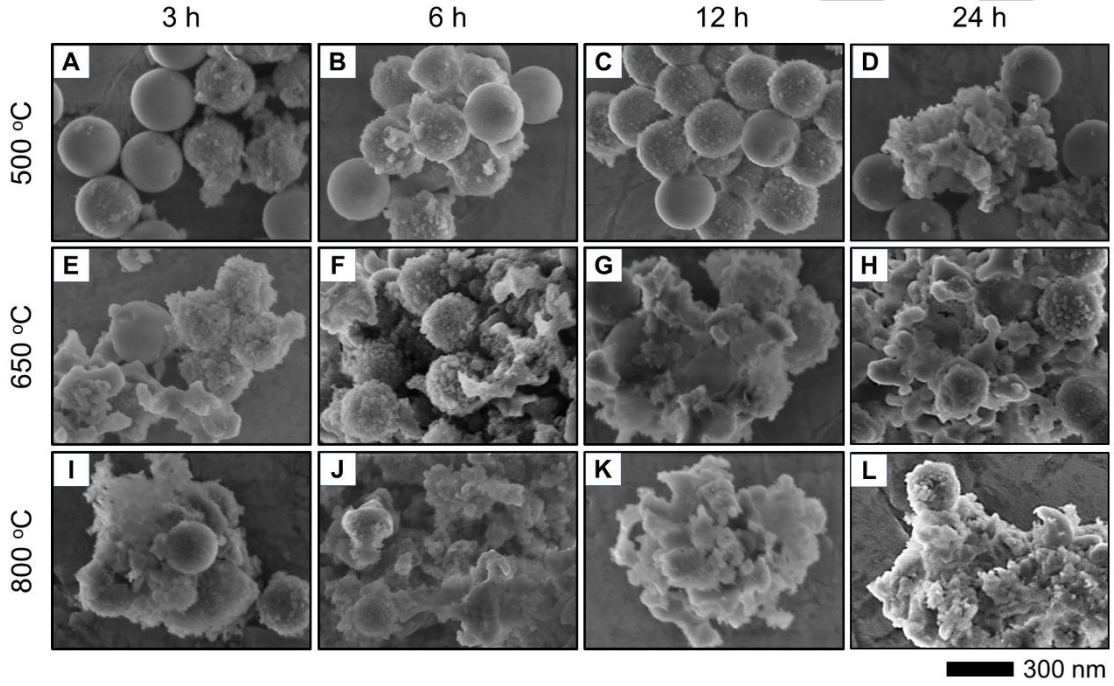

Figure 2. SEM images of Stöber silica NPs reduced with Mg at 500 °C (A-D), 650 °C (E-H), and 800 °C (I-L) for 3, 6, 12, and 24 hours.

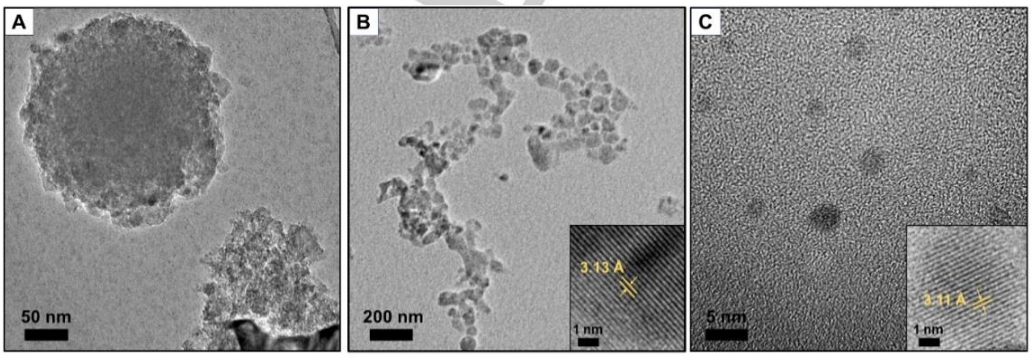

Figure 3. TEM images of (A) porous Si-NPs and (B, C) fragmented structures of porous Si obtained *via* magnesiothermic reduction at 650 °C and 12 h.

The influence of Mg grain size on the reduction reaction was also investigated. Mg fine powder (-325 mesh), chips (4 – 30 mesh), and foil (0.05 mm thickness) were used as the reductant at 650 °C for 12 h in the presence of NaCl salt. The reduction rate decreased with the increasing Mg size as evidenced by the presence of a larger SiO_2 peak in the XRD pattern (Figure S6).

Aluminothermic reduction. Similar to magnesiothermic reduction, Stöber silica NPs were mixed with -325 mesh Al powder and NaCl salt and processed at various temperatures and reaction lengths. The reaction product was treated with 10% aqueous H_3PO_4 solution to remove Al_2O_3, NaCl, and any unreacted Al. Figure 4 shows powder XRD patterns of the

10.1002/chem.201705818

resulting products. At 500 °C, a broad peak at ~22° corresponding to amorphous SiO_2 was observed for all reaction times but no crystalline Si peaks were present. The XPS results further confirmed that no elemental Si was formed at 500 °C (Figure S7). At 650 °C, which is close to the melting point of Al (660 °C), a yield of 62% elemental Si was formed after 3 h and increased to 88% after 24 h. This was further indicated in the XRD patterns of the products where reflections at 28.5°, 47.3°, and 56.1° were observed corresponding to (111), (220), and (311) crystal planes of diamond structured Si, respectively.[48] The intensity of the SiO_2 peak decreased with longer reaction length. At 800 °C, ~75% elemental Si was formed after 3 h and reached 90% after 24 h. The crystallite size at 800 °C was smaller than that obtained at 650 °C, as indicated by the increased FWHM of the XRD peaks. It is currently unclear what causes the decrease in the crystallite size; this observation will be the subject of future investigations. Reflection peaks at 35.7° and 46.0° were observed in the XRD patterns of both 650 and 800 °C processed samples, corresponding to γ-alumina.[71] These peaks remained even after 24 h of acid washing which suggests that some of the alumina is likely surrounded and protected by Si.

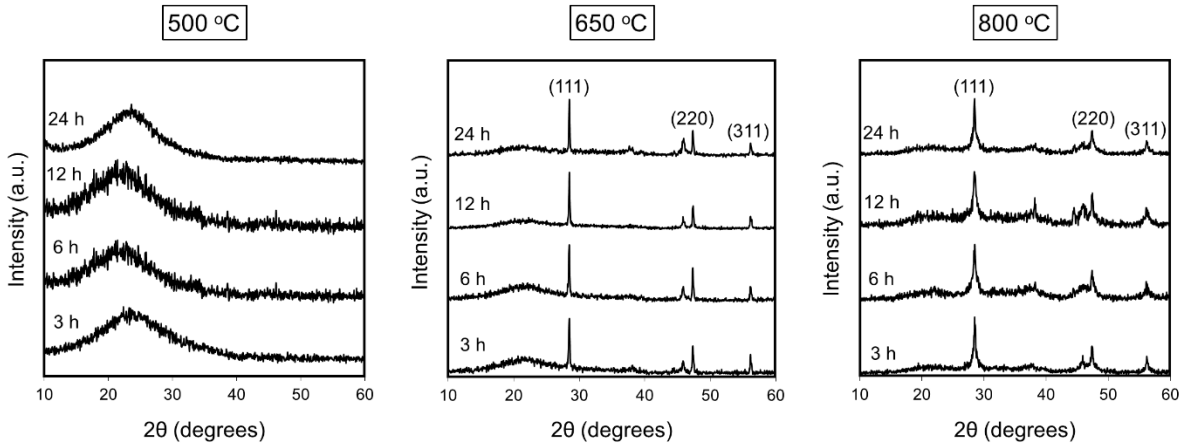

Figure 4. Powder XRD patterns of the products obtained *via* aluminothermic reduction of Stöber silica NPs at 500, 650, and 800 °C for 3, 6, 12, and 24 hours.

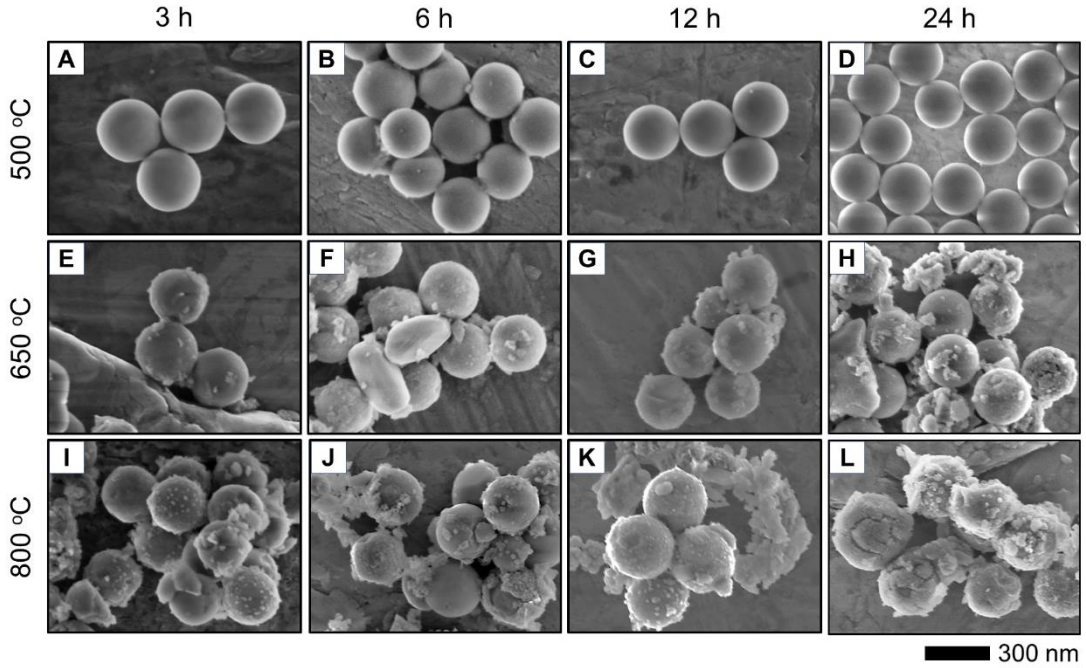

Figure 5. SEM images of Stöber silica NPs reduced with Al at 500 °C (A-D), 650 °C (E-H), and 800 °C (I-L) for 3, 6, 12, and 24 hours.

10.1002/chem.201705818

Figure 5 shows SEM images of the aluminothermic reduction products. At 500 °C, the particles are similar to the Stöber silica NPs. Some damage can be observed at 650 and 800 °C, but particle morphology was better retained in Al reduced silica NPs. It has been previously reported that the presence of alumina improves the mechanical strength of silicon formed via aluminothermic reduction.[52] The surface area of Al reduced product (Figure S8) was an order of magnitude lower compared to that of Mg. The highest surface area obtained was 37 m^2/g at 650 °C and 24 h. A pore size distribution (Figure S9) suggests pores with an average diameter of 18 nm. At 500 °C, the surface area was similar to that of silica NPs and ranged between 6.0 – 7.5 m^2/g while at 800 °C the surface area ranged between 12 – 22 m^2/g. Pore volumes of 0.07, 0.51, and 0.22 cm^3/g were obtained for Si at 500, 650, and 800 °C, respectively, after reacting for 12 hours. Figure 6A shows a TEM of porous Si-NPs obtained via aluminothermic reduction at 650 °C after 12 h reaction time. The NPs appeared to be less porous than those obtained from Mg reduction from the contrast of the electron micrographs, supporting the surface area measurements. A detailed investigation of the structural damage (Figure 6B and C) showed that the porous Si is composed of layered sheets and has a "cabbage-like" structure. There were no small nanocrystals observed in the damaged Al reduced product and only thin sheets of Si were present, as shown in Figure 6C.

The influence of Al grain size on the reduction reaction was also investigated. Al fine powder (-325 mesh), granules (~ 1 mm), and foil (0.05 mm thickness) were used as the reductant at 650 °C for 12 h in the presence of NaCl salt. No reduction product was observed in the presence of Al granules or foil (Figure S10), suggesting a high energy barrier for the nucleation process in the presence of low surface area Al.

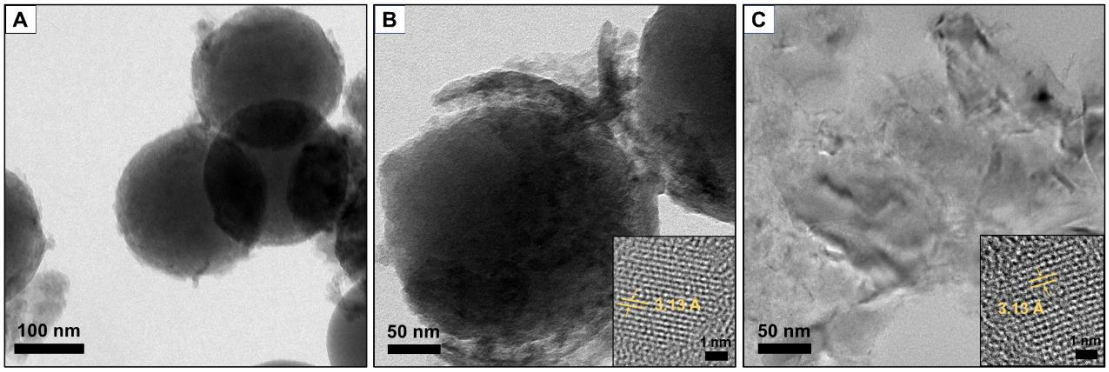

Figure 6. TEM images of porous Si-NPs and fractured structures obtained *via* magnesiothermic reduction at 650 °C and 12 h.

Calciothermic reduction. Ca metal was investigated as a reducing metal, as the calciothermic reduction of silica is thermodynamically favorable (ΔG = -168.5 kJ/mol), similar to magnesiothermic (ΔG = -135.9 kJ/mol) and aluminothermic (ΔG = -157.8 kJ/mol) reactions. Stöber silica NPs were mixed with Ca powder and NaCl salt and heated to the melting point of Ca (820 °C) for 12 h. After the reaction, the resulting product was treated with aqueous 1.0 M HCl solution. Following the reduction reactions, no Si was detected using XRD, SEM, and TEM techniques (Figure S11). This was likely due to the large size of the Ca atoms, which have a relatively high diffusion barrier that prevents the reaction from occurring.

Mixtures of Mg and Al as reductant. The Mg-Al binary phase diagram has a eutectic at 437 °C with a composition of 66.7% Mg and 33.3% Al.[72] However, eutectic mixtures have never been explored as a reductant in metallothermic reduction reactions. Since the reaction mixture also contains silica and NaCl salt, it is possible for the eutectic composition and temperature to shift. Therefore, several compositions of Mg and Al were investigated as reductant at 450 °C and 12 h reaction time (Figure 7). A 70% Mg and 30% Al mixture was found to be the most efficient reductant of all the compositions investigated using XPS. All the reduction products were found to be amorphous in nature as they lacked Si crystalline peaks in the powder XRD patterns (Figure S12).

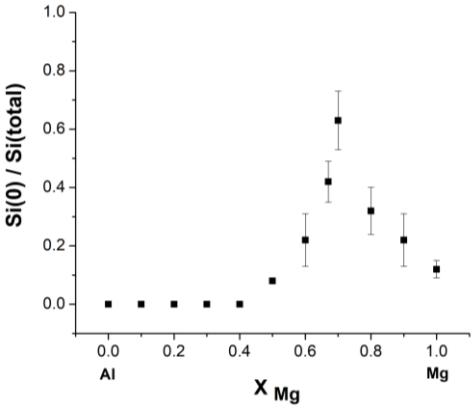

Figure 7. Formation of elemental Si (determined from XPS technique) as a function of Mg and Al composition.

10.1002/chem.201705818

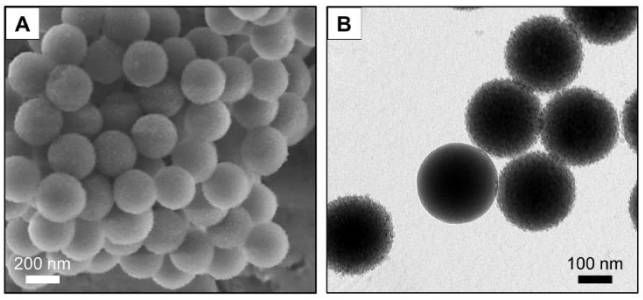

Figure 8. (A) SEM and (B) TEM images of porous Si-NPs obtained from the reduction of Stöber silica NPs with 70% Mg and 30% Al at 450 °C for 12 h.

The SEM and TEM (Figure 8) of 70% Mg and 30% Al reduced Stöber silica NPs showed minimum structural damage. HRTEM analysis showed lack of extended crystallinity in these structures consistent with the XRD analysis (Figure S13). The nanostructure of the porous Si-NP was similar to Mg reduced product and has a "blackberry-like" structure composed of smaller nanocrystals connected in 3-D. The 70% Mg/30% Al composition was further investigated as a reductant at 437 °C but only 10% of elemental Si was formed after reacting for 24 h. Porous Si-NPs obtained using 70% Mg/30% Al as the reductant had the highest surface area at 132 m^2/g (Figure S14), a pore volume of 1.0 cm^3/g, and an average pore diameter of 8 nm (Figure S15). The removal of Mg and salt byproducts was confirmed with the EDS technique (Figure S16) that showed a dominant peak originating from Si. As with the Mg reduction products, peaks from Al originating from the sample holder and O which likely arises from the Si suboxides were also observed.

The surface area and amounts of elemental Si as a function of reducing metal, time, and temperature are summarized below in Table 1.

Table 1. Summary of influence of reducing metal, temperature, and reaction length on the physical properties of porous Si-NPs.

Reducing metal	Temperature (ºC)	Time (h)	Surface area (m^2/g)	Amount of elemental Si (%)	Pore size (nm)
Mg	500	3	260 ± 30	11.2 ± 0.5	8 ± 2
Mg	500	6	391 ± 28	50.6 ± 1.8	12 ± 3
Mg	500	12	387 ± 31	71.3 ± 1.0	10 ± 3
Mg	500	24	90 ± 15	80.2 ± 1.0	12 ± 2
Mg	650	3	174 ± 22	70.8 ± 2.1	18 ± 3
Mg	650	6	200 ± 21	81.2 ± 1.8	17 ± 2
Mg	650	12	262 ± 38	88.2 ± 2.0	20 ± 4
Mg	650	24	98 ± 12	90.1 ± 2.3	20 ± 3
Mg	800	3	163 ± 15	85.3 ± 2.2	23 ± 3
Mg	800	6	170 ± 21	89.1 ± 2.4	21 ± 4
Mg	800	12	185 ± 25	90.4 ± 2.1	25 ± 3
Mg	800	24	82 ± 12	91.1 ± 2.5	26 ± 4
Al	500	3	6 ± 3	0	0
Al	500	6	6 ± 2	0	0
Al	500	12	7 ± 3	0	0
Al	500	24	7 ± 3	0	0
Al	650	3	25 ± 5	62.1 ± 1.7	12 ± 4
Al	650	6	29 ± 8	80.2 ± 2.3	15 ± 2
Al	650	12	33 ± 6	85.7 ± 2.5	18 ± 3
Al	650	24	36 ± 9	90.1 ± 2.4	18 ± 2
Al	800	3	22 ± 8	75.2 ± 2.6	20 ± 3
Al	800	6	12 ± 6	83.1 ± 2.4	19 ± 3
Al	800	12	12 ± 4	88.1 ± 2.1	21 ± 2
Al	800	24	15 ± 4	91.2 ± 2.8	20 ± 3
Ca	820	12	8 ± 3	0	0
50% Mg, 50% Al	450	12	7 ± 4	8.0 ± 1.0	7 ± 2
60% Mg, 40% Al	450	12	46 ± 7	22.0 ± 1.0	8 ± 2
67% Mg, 33% Al	450	12	102 ± 14	42.1 ± 0.7	8 ± 3
70% Mg, 30% Al	450	12	132 ± 11	63.5 ± 1.2	8 ± 1
80% Mg, 20% Al	450	12	55 ± 13	32.2 ± 1.0	7 ± 2
90% Mg, 10% Al	450	12	13 ± 4	22.0 ± 1.2	8 ± 2

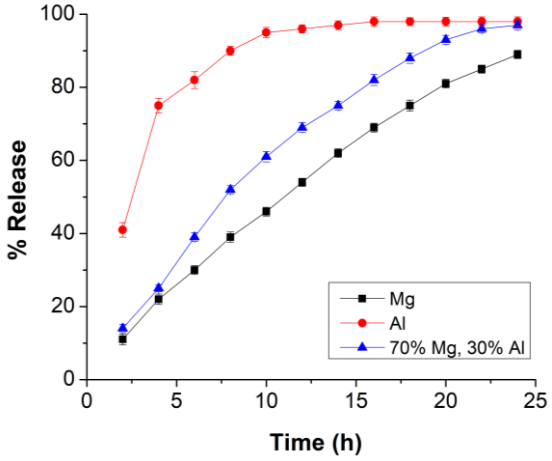

Figure 9. Release profiles of ibuprofen from porous Si-NPs obtained from the reduction of Stöber silica.

Drug loading and release. The abundance and biocompatibility[73-76] of Si combined with the porosity as demonstrated in this study makes these materials an attractive drug delivery carrier. Drug loading and release experiments with porous Si were conducted by using ibuprofen as a model drug. Drug loading was achieved using a simple immersion method where the hydrogen-terminated porous Si-NPs were stirred in hexanes containing ibuprofen for 12 hours. The loading capacities of porous Si-NPs obtained with reductants Mg, Al, and 70% Mg/30% Al were 47.2% (23.2 mmol ibuprofen/g of Si), 22.1% (10.7 mmol ibuprofen/g of Si), and 35.3% (17.1 mmol of ibuprofen/g of Si), respectively. This is consistent with the concept that higher drug loading would be expected with increased surface area and pore volume.[63] The drug release behavior of these porous Si-NPs in phosphate-buffered saline solution at pH 7.4 over 24 h is summarized in Figure 9 (% release of total loaded ibuprofen are shown in Figure S17). Porous Si-NPs obtained using Mg and 70% Mg/30% Al as reductants demonstrated a sustained release of ibuprofen over 24 hours, whereas the porous Si-NPs obtained after Al reduction had a conventional profile where ~80% of the drug was released within the first five hours. It is likely that the ibuprofen resides within the first few layers of porous Si-NPs obtained from the aluminothermic reduction which

lack a well-connected pore network, thus facilitating a faster release. However, magnesiothermic reduction results in a 3-D pore network that allows for higher drug loading and a slower release profile. This demonstrates that the reaction conditions play an important role in determining the drug loading and release behavior of porous Si.

Conclusions

In conclusion, porous Si can be synthesized *via* the solid-state reduction of Stöber silica NPs with Mg, Al, and mixtures of Mg/Al metals. Porous Si-NPs synthesized at different temperatures and reaction lengths using these metals have varying surface areas, pore volumes, and morphology retention. The grain size of the reductant metal can further determine the reaction rates. Magnesiothermic reduction yields porous Si with a "blackberry-like" structure and the highest surface area and pore volume. However, Mg also induced more structural damage at 650 and 800 °C. Aluminothermic reduction produced porous Si with the least surface area and pore volume but showed a higher degree of morphology retention. A new reductant mixture of 70% Mg and 30% Al was shown to produce porous Si at a lower temperature (450 °C) with minimal structural damage and intermediate surface area and pore volume. Porous Si-NPs obtained with different reductants were investigated as carriers for drug loading and release in phosphate-buffered saline. Porous Si obtained from Mg and a eutectic mixture of Mg and Al as reductants showed sustained release profiles whereas those made with Al as the reductant had a conventional profile. This study further demonstrates how the choice of synthetic method can influence the performance of porous Si-NPs for a given application.

Experimental Section

Materials. Tetraethyl orthosilicate (TEOS, 99.9%), ammonium hydroxide (NH_4OH, 28%), magnesium -325 mesh powder (Mg, 99.8%), and aluminum powder (Al, 99.5%) were purchased from Alfa Aesar. Calcium (Ca, 99%), phosphate buffered saline (pH 7.4), ibuprofen (≥ 98%), magnesium chips (Mg, 99.98%), magnesium foil (Mg, 99.9%), aluminum granules (Al, 99.7%), aluminum foil (Al, 98%), dialysis sacks and phosphoric acid solution (H_3PO_4, 85%) were purchased from Sigma-Aldrich. Sodium chloride (NaCl, 99%) was purchased from Chimiques ACP Chemicals Inc. Hydrochloric acid (HCl, 36.5-38.0%) was purchased from Anachemia. Water (≥18.2 MΩ cm resistivity) was obtained from a Barnstead E-Pure system. All the reagents were used as received without further purification.

Synthesis of Stöber silica NPs. 3.00 mL of 28% NH_4OH was added to 50.0 mL of 95% EtOH and stirred together for 5 min, followed by the addition of 1.50 mL of TEOS. The reaction was stirred at 18 °C for 12 h (ambient humidity was recorded to be 82%). The silica product was collected by centrifuging at 3300 rpm for 15 min. The solid white product was washed three times with EtOH and dried overnight in an oven at 80 °C.

Metallothermic reduction of Stöber silica NPs. In a typical reduction reaction, 0.20 g of Stöber silica NPs (4.16 mmol) was mixed using a spatula with a 2.10 (Mg and Ca) or 1.50 (Al) molar excess of the metal along with NaCl salt (1.00 g). The mixture was transferred to a ceramic reaction boat and annealed under an Ar atmosphere at a predetermined temperature and time, with a heating rate of 10 °C/min. The reaction product was treated with 1.00 M HCl solution (25.0 mL) for 4 h when Mg and Ca were used as the reducing metals. The reaction product was treated with 10% aqueous H_3PO_4 solution (25.0 mL) for 4 h when Al was used as the reductant. The solid product was collected by centrifuging at 3000 rpm for 15 min. The product was then washed twice with DI-water (15.0 mL) and once with acetone (15.0 mL) and dried overnight in the oven at 80 °C. Mixtures of Mg and Al metals were also investigated as reductants for silica NPs. A mixture of Stöber silica NPs, reductant, and NaCl was transferred to a ceramic reaction boat and annealed under an Ar atmosphere at a predetermined temperature and time at a heating rate of 10 °C/min. The product was sequentially washed with 1.0 M HCl (25.0 mL) and 10% aqueous H_3PO_4 solution (25.0 mL), respectively, for 4 h in each solution.

Drug loading and release. Si-NPs (25 mg) were treated with 10 mL of 49% hydrofluoric acid solution for 15 min and collected *via* centrifugation. On average ~15 mg of the hydride terminated porous Si was recovered after the etching reaction. They were immediately stirred in 30 mg/mL ibuprofen hexane solution (5.00 mL) for 12 h in a sealed vial. The NPs were collected by centrifuging at 3000 rpm and washed with hexanes three times. The drug loading was determined by analyzing the concentration of ibuprofen in the supernatant and washed solutions using an ultraviolet-visible (UV-Vis) spectrophotometer. For the release studies, a dialysis sack with a molecular weight cut-off from 8000 – 14,000 Da was filled with drug loaded Si-NPs dispersed in PBS solution (pH = 7.4). The dialysis sack was placed in 50.0 mL of PBS solution stirring at 37 °C. The solution outside of the dialysis sack was analyzed using UV-Vis spectroscopy to determine the diffused ibuprofen concentration. The loading capacities are reported in the % weight of the ibuprofen in the original stock solution transferred to the porous Si-NP.

Characterization methods. Powder X-ray powder diffraction (XRD) patterns were collected using a Rigaku Ultima IV X-Ray diffractometer with CuKα radiation (λ = 1.54 Å). The samples were placed on to a zero-background Si wafer and the spectra were collected at 3 counts/s. Scanning electron micrographs (SEM) were obtained on a Hitachi S-4700 electron microscope. The substrates were cleaned with piranha solution prior to sample deposition. The samples were drop casted from a water dispersion. were Energy-dispersive X-ray spectra (EDS) were collected in the scanning-electron microscope (SEM) at an accelerating voltage of 15 kV using a silicon drift detector. The samples were analyzed using Image J software (version 1.45). Transmission electron micrographs (TEM) using an FEI Tecnai F30ST microscope with an accelerating voltage of 300 kV. TEM samples were prepared by drop coating the nanoparticle suspension onto a carbon coated copper grid with a 400 µm diameter hole. The NC size was determined using Image J software (version 1.45). Brunauer-Emmett-Teller (BET) surface area measurements were performed on a Micromeritics Flowsorb II 2300 BET surface area analyser. DFT pore size distributions were calculated using a cylindrical pore on an oxide surface and a N_2 probe gas. The DFT fits were optimized such that the roughness of the distribution was minimized without significantly increasing the error. X-ray photoelectron spectroscopy (XPS) analyses were performed using a Kratos Axis Ultra instrument operating in energy spectrum mode at 210 W. The base pressure and operating chamber pressure were maintained at 10^{-7} Pa. A monochromatic Al K_α source (λ = 8.34 Å) was used to irradiate samples, and spectra were obtained with an electron takeoff angle of 90°. To minimize sample charging the charge neutralizer filament was used as appropriate. Survey spectra were collected using an elliptical spot with major and minor axis lengths of 2 and 1 mm, respectively, and 160 eV pass energy with a step of 0.33 eV. CasaXPS software (VAMAS) was used to interpret high-resolution (HR) XP spectra. All spectra were internally

calibrated to the C 1s emission (284.8 eV). After calibration, the background was subtracted using a Shirley-type background to remove most of the extrinsic loss structure. The full width at half maximum (FWHM) for all the fitted peaks was maintained below 1.2 eV. Since XPS is a surface sensitive technique, the particles were pulverized to produce 5 – 8 nm structures to allow for complete X-ray penetration through the NP.

Acknowledgements

The authors acknowledge funding from the Natural Sciences and Engineering Research Council of Canada (NSERC), Canada Foundation for Innovation (CFI), and Dalhousie University. Patricia Scallion and Clean Technologies Research Institute are thanked for access and assistance with the SEM analysis. Drs. Jeff Dahn and Xiaowei Ma are thanked for assistance with the BET analysis. The staff at the Alberta Centre for Surface Engineering and Sciences (ACSES) is thanked for XPS analysis.

Keywords: Nanomaterials • porous silicon• solid-state synthesis • drug delivery • biocompatible

[1] N. A. Krueger, A. L. Holsteen, S. K. Kang, C. R. Ocier, W. Zhou, G. Mensing, J. A. Rogers, M. L. Brongersma, P. V. Braun, *Nano Lett*. **2016**, *16*, 7402-7407.

[2] C. R. Ocier, N. A. Krueger, W. Zhou, P. V. Braun, *ACS Photonics* **2017**, *4*, 909.

[3] V. V. Pellegrini, A. Tredicussi, C. Mazzoleni, L. Pavesi, *Phys. Rev. B* **1995**, *52*, 14328-14331.

[4] A. G. Cullis, L. T. Canham, P. D. J. Calcott, *J. Appl. Phys*. **1997**, *82*, 909-965.

[5] W. Thieb, *Surf. Sci. Rep*. **1997**, *29*, 91-192.

[6] V. Torres-Costa, R. J. Martin-Palma, *J. Mater. Sci*. **2010**, *45*, 2823-2838.

[7] E. J. Anglin, L. Cheng, W. R. Freeman, M. J. Sailor, *Adv. Drug Deliv. Rev*. **2008**, *60*, 1266-1277.

[8] S. J. P. McInnes, E. J. Szili, S. A. Al-Bataineh, R. B. Vasani, J. Xu, M. E. Alf, K. K. Gleason, R. D. Short, N. H. Voelcker, *Langmuir* **2016**, *32*, 301-308.

[9] H. Alhmound, B. Delatat, R. Elnathan, A. Cifuentes-Rius, A. Chaix, M. Rogers, J. Durand, N. H. Voelcker, *Adv. Funct. Mater*. **2015**, *25*, 1137-1145.

[10] S. M. Haidary, E. P. Corcoles, N. K. Ali, J. Nanomater. 2012, 830503.

[11] A. Venuta, J. Wolfram, H. Shen, M. Ferrari, J. *Mater. Chem. B* **2017**, *5*, 207-219.

[12] I. A. Levitsky, *Sensors* **2015**, *15*, 19968-19991.

[13] F. A. Harraz, *Sensor Actuat. B* **2014**, *202*, 897-912.

[14] C. Pacholski, *Sensors* **2013**, *13*, 4694-4713.

[15] S. Dhanekar, S. Jain, *Biosens. Bioelectron*. **2013**, *41*, 54-64.

[16] M. J. Sailor, E. C. Wu, *Adv. Funct. Mater*. **2009**, *19*, 3195-3208.

[17] A. Jane, R. Dronov, A. Hodges, N. H. Voelcker, *Trends Biotechnol*. **2009**, *27*, 230-239.

[18] L. N. Acquaroli, T. Kuchel, N. H. Voelcker, *RSC Adv*. **2014**, *4*, 34768-34773.

[19] A. I. Manilov, V. A. Skryshevsky, *Mater. Sci. Eng. B* **2013**, *178*, 942-955.

[20] P. Kale, A. C. Gangal, R. Edla, P. Sharma, *Int. J. Hydrogen Energ*. **2012**, *37*, 3741-3747.

[21] M. Ge, X. Fang, J. Rong, C. Zhou, *Nanotechnology* **2013**, *24*, 422001.

[22] X. Su, Q. Wu, J. Li, X. Xiao, A. Lott, W. Lu, B. W. Sheldon, J. Wu, *Adv. Energy Mater*. **2014**, *4*, 1300882.

[23] M. Ashuri, Q. He, L. L. Shaw, *Nanoscale* **2016**, *8*, 74-103.

[24] M. Ge, J. Rong, X. Fang, A. Zhang, Y. Lu, C. Zhou, *Nano Res*. **2013**, *6*, 174-181.

[25] H. Song, D. Liu, J. Yang, L. Wang, H. Xu, Y. Xiong, *ChemNanoMat* **2017**, *3*, 22-26.

[26] F. Dai, J. Zai, R. Yi, M. L. Gordin, H. Sohn, S. Chen, D. Wang, *Nat. Commun*. **2014**, *5*, 3605.

[27] N. R. Mathews, P. J. Sebastian, X. Mathew, V. Agarwal, *Int. J. Hydrogen Energ*. **2003**, *28*, 629-632.

[28] M. Dasog, S. Kraus, R. Sinelnikov, J. G. C. Veinot, B. Rieger, *Chem. Commun*. **2017**, *53*, 3114-3117.

[29] A. G. Cullis, L. T. Canham, *Nature* **1991**, *353*, 26-28.

[30] V. Lehmann, H. Foll, *J. Electrochem. Soc*. **1990**, *137*, 653-659.

[31] R. L. Smith, S. D. Collins, *J. Appl. Phys*. **1992**, *71*, R1-R22.

[32] Z. Huang, N. Geyer, P. Werner, J. de Boor, U. Gosele, *Adv. Mater*. **2011**, *23*, 285-308.

[33] Z. Huang, T. Shimizu, S. Senz, Z. Zhang, N. Geyer, U. Gosele, *J. Phys. Chem. C* **2010**, *114*, 10683-10690.

[34] A. Esmanski, G. A. Ozin, *Adv. Funct. Mater*. **2009**, *19*, 1999-2000.

[35] C. R. Miranda, A. F. Azevedo, M. R. Baldan, A. F. Beloto, N. G. Ferreira, *J. Nanosci. Nanotechnol*. **2009**, *9*, 3877-3882.

[36] M. Nagamori, I. Malinsky, A. Claveau, *Metall. Trans. B* **1986**, *17*, 503-514.

[37] Z. Bao, M. R. Weatherspoon, S. Shian, Y. Cai, P. D. Graham, S. M. Allan, G. Ahmad, M. B. Dickerson, B. C. Church, Z. Kang, H. W. Abernathy III, C. J. Summers, M. Liu, K. H. Sandhage, *Nature* **2007**, *446*, 172-175.

[38] E. K. Richman, C. B. Kang, T. Brezesinski, S. H. Tolbert, *Nano Lett*. **2008**, *8*, 3075-3079.

[39] K. H. Kim, D. J. Lee, K. M. Cho, S. J. Kim, J. K. Park, H. T. Jung, *Sci. Rep*. **2015**, *5,* 9014.

[40] N. Lin, Y. Han, J. Zhou, K. Zhang, T. Xu, Y. Zhu, Y. Qian, *Energy Environ. Sci*. **2015**, *8*, 3187-3191.

[41] Z. W. Zhou, Y. T. Liu, X. M. Xie, X. Y. Ye, *Chem. Commun*. **2016**, *52*, 8401-8404.

[42] S. Choi, T. Bok, J. Ryu, J. I. Lee, J. Cho, S. Park, *Nano Energy* **2015**, *12*, 161-168.

[43] D. P. Wong, H. T. Liean, Y. T. Chen, K. H. Chen, L. C. Chen, *Green Chem*. **2012**, *14*, 896-900.

[44] Z. Favors, W. Wang, H. H. Bay, Z. Mutlu, K. Ahmed, C. Liu, M. Ozkan, C. S. Ozkan, *Sci. Rep*. **2014**, *4*, 5623.

[45] N. H. Hai, I. Grigoriants, A. Gedanken, *J. Phys. Chem. C* **2009**, *113*, 10521-10526.

[46] W. S. Kim, Y. Hwa, J. H. Shin, M. Yang, H. J. Sohn, *Nanoscale* **2014**, *6*, 4297-4302.

[47] J. K. Yoo, J. Kim, M. Choi, Y. U. Park, J. Hong, K. M. Baek, K. Kang, Y. S. Jung, *Adv. Energ. Mater*. **2014**, *4*, 1400622.

[48] M. Dasog, Z. Yang, J. G. C. Veinot, *CrystEngComm* **2012**, *14*, 7576-7578.

[49] M. P. Liu, C. H. Li, H. B. Du, X. Z. You, *Chem. Commun*. **2012**, *48*, 4950-4952.

[50] M. Guo, X. Zou, H. Ren, F. Muhammad, C. Huang, S. Qiu, G. Zhu, *Micropor. Mesopor. Mat*. **2011**, *142*, 194-201.

[51] K. Shinoda, H. Murakami, Y. Sawabe, K. Saegusa, *Chem. Eng. J.* **2012**, *198*, 61-64.

[52] T. D. Nguyen, W. Y. Hamad, M. J. MacLachlan, *Chem. Mater*. **2016**, *28*, 2581-2588.

[53] S. Inasawa, Y. Ono, T. Mizuguchi, A. Sunairi, S. Makamura, Y. Tsuji, Y. Yamaguchi, *CrystEngComm* **2017**, *19*, 2681-2686.

[54] P. Shen, N. Uesawa, S. Inasawa, Y. Yamaguchi, *Langmuir* **2010**, *26*, 13522-13527.

[55] J. L. Dye, K. D. Cram, S. A. Urbin, M. Y. Redko, J. E. Jackson, M. Lefenfeld, *J. Am. Chem. Soc*. **2005**, *127*, 9338-9339.
[56] L. Lin, X. Xu, C. Chu, M. K. Majeed, J. Yang, *Angew. Chem. Int. Ed*. **2016**, *55*, 14063-14066.
[57] H. Maruyama, H. Nakano, M. Ogawa, M. Nakamoto, T. Ohta, A. Sekiguchi, *Sci. Rep*. **2015**, *5*, 13219.
[58] S. Murugesan, J. T. Harris, B. A. Korgel, K. J. Stevenson, *Chem. Mater*. **2012**, *24*, 1306-1315.
[59] Z. Kang, C. H. A. Tsang, N. B. Wong, Z. Zhang, S. T. Lee, *J. Am. Chem. Soc*. **2007**, *129*, 12090-12091.
[60] F. Erogbogbo, T. Lin, P. M. Tucciarone, K. M. LaJoie, L. Lai, G. D. Patki, P. N. Prasad, M. T. Swihart, *Nano Lett*. **2013**, *13*, 451-456.
[61] G. A. Tritsaris, E. Kaxiras, S. Meng, E. Wang, *Nano Lett*. **2013**, *13*, 2258-2263.
[62] Z. Xie, Z. Ma, Y. Wang, Y. Zhou, C. Lu, *RSC Adv*. **2016**, *6*, 22383-22388.
[63] N. H. Maniya, S. R. Patel, Z. V. P. Murthy, *Rev. Adv. Mater. Sci*. **2016**, *44*, 257-272.
[64] P. A. Kulyavtsev, R. P. Spencer, *Pharm. Pat. Anal*. **2017**, *6*, 77-85.
[65] S. J. P. McInnes, T. D. Michl, B. Delalat, S. A. Al-Bataineh, B. R. Coad, K. Vasilev, H. J. Griesser, N. H. Voelcker, *ACS Appl. Mater. Interfaces* **2016**, *8*, 4467-4476.
[66] N. L. Fry, G. R. Boss, M. J. Sailor, *Chem. Mater*. **2014**, *26*, 2758-2764.
[67] K. Nozawa, H. Gailhanou, L. Raison, P. Panizza, H. Ushiki, E. Sellier, J. P. Delville, M. H. Delville, *Langmuir* **2005**, *21*, 1516-1523.
[68] W. C. Cho, H. J. Kim, H. I. Lee, M. W. Seo, H. W. Ra, S. J. Yoon, T. Y. Mun, Y. K. Kim, J. H. Kim, B. H. Kim, *Nano Lett*. **2016**, *16*, 7261-7269.
[69] W. Luo, X. Wang, C. Meyers, N. Wannenmacher, W. Sirisaksoontorn, M. M. Lerner, X. Ji, *Sci. Rep*. **2013**, *3*, 2222.
[70] A. Khawam, D. R. Flanagan, *J. Phys. Chem. B* **2006**, *100*, 17315-17328.
[71] G. Paglia, C. E. Buckley, A. L. Rohl, R. D. Hart, K. Winter, A. J. Studer, B. A. Hunter, J. V. Hanna, *Chem. Mater*. **2004**, *16*, 220-236.
[72] M. Mezbahul-Islam, A. O. Mostafa, M. Medraj, *J. Mater*. **2014**, 704283.
[73] S. K. Kang, G. Park, K. Kim, S. W. Hwang, H. Cheng, J. Shin, S. Chung, M. Kim, L. Yin, J. C. Lee, *ACS Appl. Mater. Interfaces* **2015**, *7*, 9297-9305.
[74] S. P. Low, N. H. Voelcker, L. T. Canham, K. A. Williams, *Biomaterials* **2009**, *30*, 2873-2880.
[75] A. F. G. Leontowich, C. F. Calver, M. Dasog, R. W. J. Scott, *Langmuir* **2009**, *26*, 1285-1290.
[76] L. M. Bimbo, M. Sarparanta, H. A. Santos, A. J. Airaksinen, E. Makila, T. Laaksonen, L. Peltonen, V. P Lehto, J. Hirvonen, J. Salonen, *ACS Nano* **2010**, *4*, 3023-3032.

10.1002/chem.201705818

WILEY-VCH

Entry for the Table of Contents (Please choose one layout)

Layout 2:

FULL PAPER

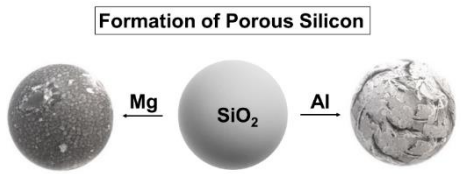

*Author(s), Corresponding Author(s)**

Page No. – Page No.

Title